Effect of annealing ambient on anisotropic retraction of film edges during solid-state dewetting of thin single crystal films

Gye Hyun Kim, Wen Ma, Bilge Yildiz, and Carl V. Thompson'

Citation: J. Appl. Phys. **120**, 075306 (2016); doi: 10.1063/1.4961205
View online: http://dx.doi.org/10.1063/1.4961205
View Table of Contents: http://aip.scitation.org/toc/jap/120/7
Published by the American Institute of Physics

Effect of annealing ambient on anisotropic retraction of film edges during solid-state dewetting of thin single crystal films

Gye Hyun Kim,[1] Wen Ma,[2] Bilge Yildiz,[1,2] and Carl V. Thompson[1,a)]
[1]*Department of Materials Science and Engineering, Massachusetts Institute of Technology, Cambridge, Massachusetts 01239, USA*
[2]*Department of Nuclear Science and Engineering, Massachusetts Institute of Technology, Cambridge, Massachusetts 01239, USA*

(Received 4 June 2016; accepted 4 August 2016; published online 18 August 2016)

During solid-state dewetting of thin single crystal films, film edges retract at a rate that is strongly dependent on their crystallographic orientations. Edges with kinetically stable in-plane orientations remain straight as they retract, while those with other in-plane orientations develop in-plane facets as they retract. Kinetically stable edges have retraction rates that are lower than edges with other orientations and thus determine the shape of the natural holes that form during solid-state dewetting. In this paper, measurements of the retraction rates of kinetically stable edges for single crystal (110) and (100) Ni films on MgO are presented. Relative retraction rates of kinetically stable edges with different crystallographic orientations are observed to change under different annealing conditions, and this accordingly changes the initial shapes of growing holes. The surfaces of (110) and (100) films were also characterized using low energy electron diffraction, and different surface reconstructions were observed under different ambient conditions. The observed surface structures were found to correlate with the observed changes in the relative retraction rates of the kinetically stable edges. *Published by AIP Publishing*. [http://dx.doi.org/10.1063/1.4961205]

I. INTRODUCTION

When solid thin films are heated, they often dewet or agglomerate to form islands at temperatures well below the film's melting temperature. Dewetting is driven by surface and interface energy minimization and typically occurs through capillary-driven atomic self-diffusion on the free surfaces of the films.[1] The driving force and rate of dewetting increases as the film thickness is decreased and when increasingly small features are patterned from films. As a consequence, as film and feature sizes have been decreased due to size scaling of micro- and nano-systems, such as integrated circuits,[2–4] suppression of dewetting during processing and operation has become an increasing challenge. At the same time, complete or controlled partial dewetting has come to be recognized as a means of producing arrays of micro- and nano-structured features for applications in a variety of devices and systems, including sensors,[5,6] plasmonic devices,[7–9] solar cells,[10,11] and photocatalyic systems.[12] To either suppress or use dewetting, improved understandings of the mechanisms that govern capillary-driven anisotropic morphological evolution are needed.

Solid-state dewetting proceeds through the motion of three-phase boundaries at which the film, substrate, and ambient meet. These triple-phase lines are found at substrate edges or around naturally forming holes in the film. They can also be the result of lithographic patterning of films.[1] Once three-phase boundaries are present, dewetting proceeds by curvature-driven surface diffusion away from the three-phase boundaries and results in the movement of the boundaries, in the form of retraction of the edges of the film. Thickening rims form on retracting edges due to local differences in the diffusion flux,[1,13,14] and valleys sometimes form ahead of the retracting rims.[1,13–16]

In single crystal films, the retraction rate of an edge depends on the out-of-plane orientation of the film and the in-plane orientation of the edge. This has been observed to affect the initial shapes of holes growing in single crystal films of Si,[17–20] Ni,[21,22] and Au-Fe[23] and of patterned edges of Ni[22] and Si[24] films. Ye and Thompson[22] studied the solid state dewetting of Ni films patterned into large patches with initially straight macroscopic edges aligned with different in-plane orientations. For films with a specific crystallographic direction normal to the plane of the film, i.e., texture, edges with specific in-plane orientations were found to remain straight as they retracted. Such edges are referred to as kinetically stable edges. The rates of retraction of kinetically stable edges are lower than those of the edges with other nearby orientations so that the retraction rate of kinetically stable edges is locally minimum with respect to changes in the in-plane orientation of the edge. Edges with other in-plane orientations develop periodic in-plane facets, with each facet having a kinetically stable orientation. When holes form and grow in a single crystal film, they are initially bound by kinetically stable edges. For example, in Ni films with (100) texture, holes initially have square shapes and are bound by edges that retract in ⟨110⟩ or ⟨010⟩ directions, and in Ni (110) films, holes initially have rectangular shapes bound by edges that retract in ⟨100⟩ and ⟨110⟩ directions[22] (see the insets in Figure 1). This phenomenology clearly indicates that crystalline anisotropy plays a critical role in defining the rate of edge retraction and the overall dewetting rate of a

a)Author to whom correspondence should be addressed. Electronic mail: cthomp@mit.edu

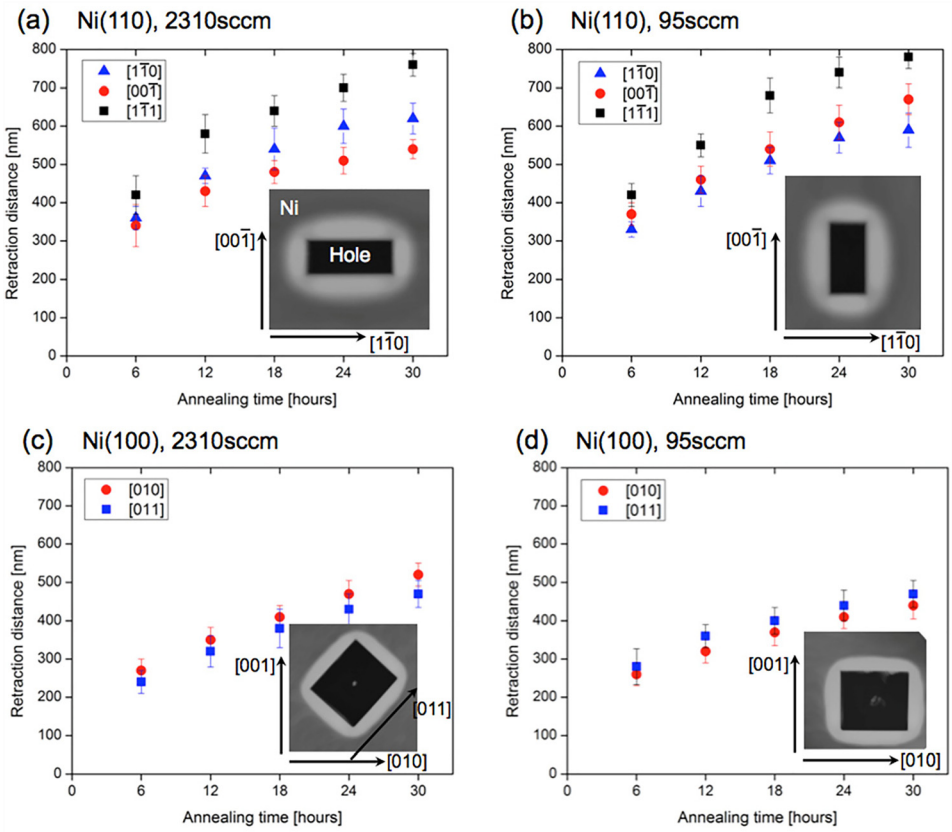

FIG. 1. (a) and (c) Retraction distance versus annealing time with 5% H_2 + 95% N_2 flowing at a rate of 2310 sccm. (b) and (d) Retraction distance versus annealing time with 5% H_2 + 95% N_2 flowing at a rate of 95 sccm. The out-of-plane orientation of the Ni film and the in-plane retraction directions are indicated in each figure. The inset images are AFM images of natural holes under each experimental condition. Corresponding in-plane directions are indicated with the images.

film. The anisotropy of both surface energies and surface self-diffusivities can affect the rate of edge retraction.

Ye and Thompson[22] observed that the shape of a natural hole, defined by the kinetically stable edges with locally minimum retraction rates, can be different under different annealing conditions, as illustrated in Figure 1. The annealing ambient has also been observed to affect the phenomenology of solid-state dewetting of polycrystalline films.[25–27] This indicates that the relative retraction rates for edges with different crystallographic orientations are affected by ambient conditions. Zucker *et al.*[28] developed a simulation for the retraction of fully facetted kinetically stable edges and investigated the relative effects of surface energy anisotropy and surface diffusivity anisotropy on the rate of edge retraction. By varying the relative surface energy and diffusivity of individual facets, they found that surface diffusivity anisotropy has a greater impact on the retraction rate than the surface energy anisotropy. Furthermore, it was found that the surface diffusivity on the top facet of the retracting rim most strongly affects the dewetting kinetics. It is also known[29–31] that differences in the annealing gas composition can lead to different surface reconstructions associated with different adsorbed gases. Surface reconstructions can significantly change surface diffusivities. It therefore seems likely that changes in ambient annealing conditions might change edge retraction rates due to changes in surface structures.

In this paper, analyses of the kinetics of retraction of kinetically stable edges in Ni(100) and Ni(110) films are reported. Corresponding changes in surface structures have also been observed using low energy electron diffraction (LEED) and are found to be correlated with changes in the anisotropy of edge retraction rates.

II. EXPERIMENTAL PROCEDURES

130 nm-thick single crystal Ni(110) and Ni(100) films were deposited on polished single-crystal (110) and (100) MgO substrates (purchased from MTI Corporation) using electron beam deposition. The as-deposited films were patterned using optical photolithography with SPR 700 positive photoresist and CD 26 developer followed by wet etching of Ni in 69% HNO_3, H_2SO_4, CH_3COOH, and H_2O with a volume ratio of 7.2:2:5:28. After patterning, the remaining photoresist was removed using acetone and then ultrasonicated in RR41 (dimethyl sulfoxide-based photoresist remover). Additional details of the film deposition and the patterning procedures are available elsewhere.[16] Annealing of the patterned films was conducted in a tube furnace at 700 °C with reducing gas (5% H_2 and 95% N_2) flowing at rates of 2310 sccm or 95 sccm, or with another reducing gas (2% H_2 and 98% Ar) flowing at a rate of 390 sccm. These reducing gases are expected to remove nickel oxide from the Ni surface and prevent oxidation during edge retraction. The oxygen concentration in the furnace was measured during annealing using an Accucarb oxygen measurement probe. Some samples were also annealed with pure Ar flowing at a rate of 2310 sccm to measure the partial pressure of oxygen without the presence of H_2. Scanning electron microscopy in an FEI/Philips XL30 FEG ESEM was used for measurements of retraction

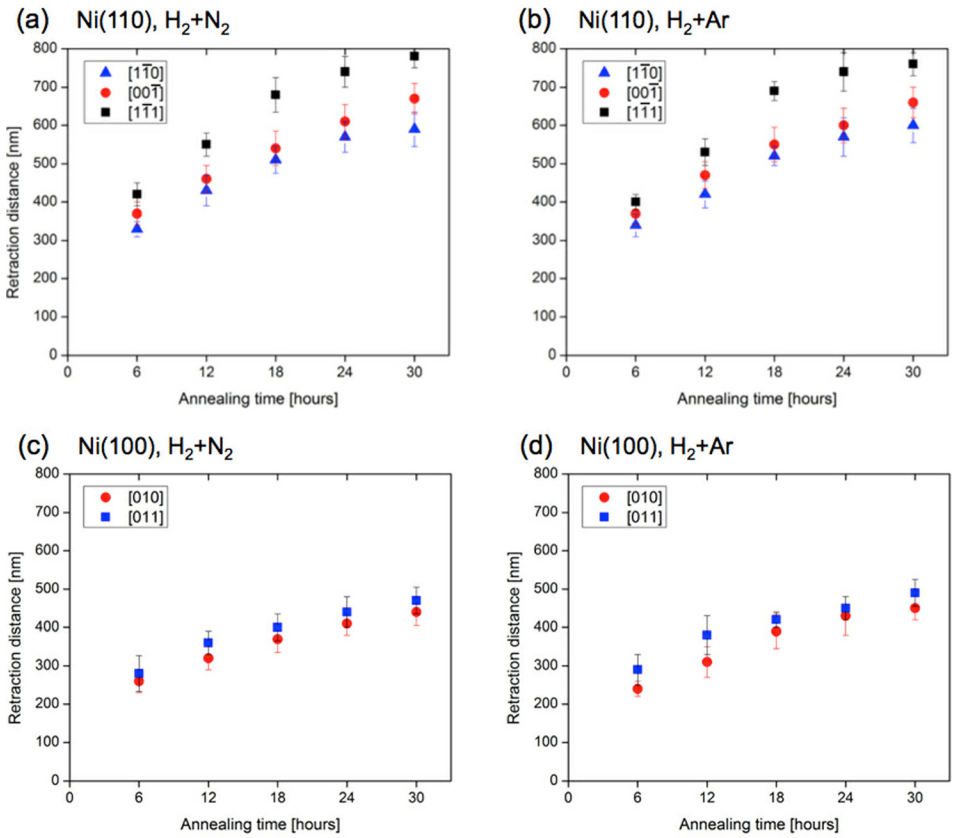

FIG. 2. (a) and (c) Retraction distance versus annealing time with 5% H_2 + 95% N_2 flowing at a rate of 95sccm. (b) and (d) Retraction distance versus annealing time with 2% H_2 + 98% Ar flowing at a rate of 390 sccm. Under these flow rates, the same partial pressure of oxygen was measured. The out-of-plane orientation of the Ni film and the in-plane retraction directions are indicated in each figure.

distances. AFM imaging was conducted using a Veeco Nanoscope IV AFM in tapping mode. A focused ion beam (Helios Dual Beam Workstation) was used to make cross-sections for SEM imaging of the rims at edges.

Low energy electron diffraction (LEED) was used in a separate UHV system to characterize the surface structure of Ni(110) and Ni(100) films annealed at 700 °C in different annealing ambient conditions. Once a sample was loaded in the chamber and the chamber was pumped to a base pressure of low 10^{-9} Torr, the surface oxide was cleaned using Ar bombardment with an Ar pressure of 5×10^{-6} Torr at an accelerating voltage of 2 kV for 1 h. After the cleaning, the samples were annealed under vacuum at 500 °C for 1 h to heal the surface and desorb the Ar. The samples were then heated to 700 °C and H_2 or O_2 was introduced to the entire chamber to a pressure of 1×10^{-7} Torr for 10 s, while LEED patterns were collected using a filament current of 2.7 A and an emission current of 300 μA.

III. RESULTS

Figure 1 shows the measurements of retraction distances versus annealing time for kinetically stable edges for Ni(110) and Ni(100) films under 5% H_2 + 95% N_2 flowing at a rate of 2310 sccm or 95 sccm. These measurements can be used to calculate the edge retraction rates. It can be seen that changes in the reducing gas flow rate result in clear changes in the relative retraction distances over time for ⟨110⟩ and ⟨100⟩ edges in both Ni(110) and Ni(100) films.

Edge retraction distances were measured after different annealing times, and it was found that the retraction distance roughly scaled with $\sim t^{0.4}$. This is consistent with more detailed experiments on samples that were identically prepared and tested, as reported in an earlier study.[16] This result is also consistent with a number of modeling results.[1,14,28]

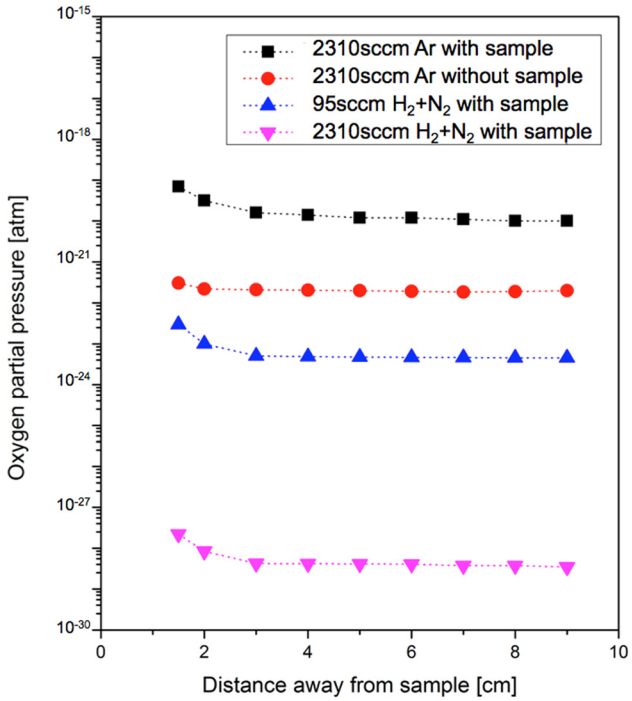

FIG. 3. Oxygen partial pressure profiles along the tube furnace under different annealing conditions. Due to the physical constraints of the oxygen probe, the closest distance away from the sample surface the probe could be used was 1.5 cm.

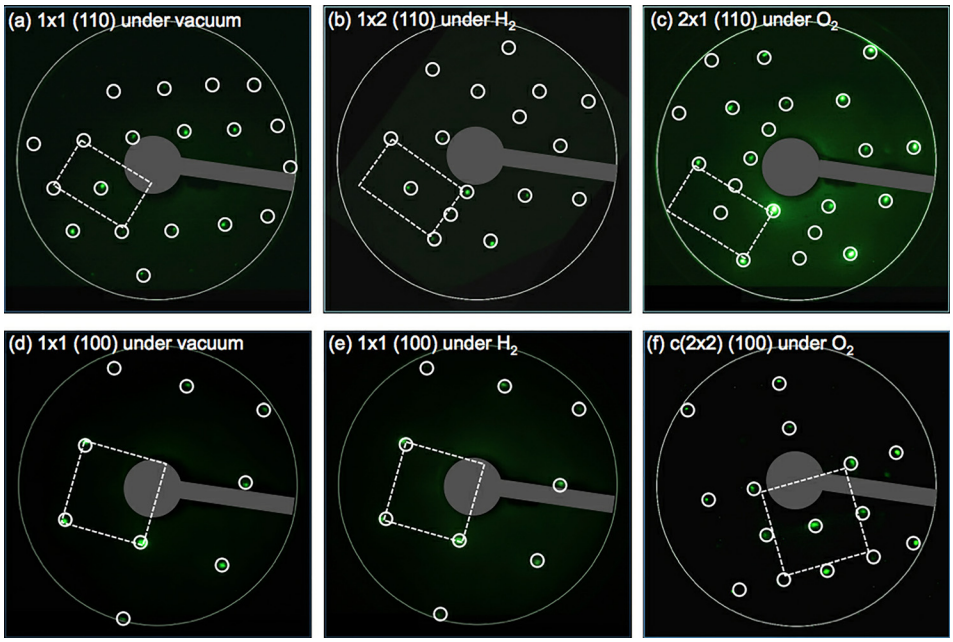

FIG. 4. LEED patterns for Ni(110) and Ni(100) surfaces collected in vacuum or under low pressures of H_2 or O_2. Specific ambient conditions are indicated in Table I. The patterns in the first row ((a)–(c)) are for (110) surfaces and those in the second row ((d)–(f)) are for (100) surfaces. White circles are drawn as visual aids to indicate the diffraction spots. White dashed lines indicate the unit cells of surface structures. Some diffraction spots are not visible because the electron source blocks the screen.

Figure 2 shows retraction distance measurements for kinetically stable edges in Ni(110) and Ni(100) films versus annealing time in 5% H_2 + 95% N_2 flowing at a rate of 95 sccm and in 2% H_2 + 98% Ar flowing at a rate of 390 sccm. The oxygen pressure was found to be the same under both conditions (4.5×10^{-24} atm). It can be seen that there is no significant difference in the retraction distances; thus, it can be concluded that changes in the partial pressures of N_2 or Ar are not responsible for the changes observed under different reducing gas flow conditions.

Figure 3 shows the oxygen partial pressure profiles along the tube furnace under different annealing conditions. Under a fixed flow rate of pure Ar, there was a partial pressure difference of about two orders of magnitude when the samples were present in the furnace and when they were not. This indicates that the MgO substrate was a significant source of oxygen during annealing. The calculated equilibrium vapor pressure for O_2 over MgO at 1200 K is about 10^{-15} atm.[32] Given that the O_2 partial pressure in our experiments is significantly lower than this, it seems likely that congruent vaporization of MgO to form gaseous O_2 has occurred.

To analyze the effect of H_2 and O_2 on the surface structure of Ni(110) and Ni(100), LEED was used and the results are illustrated in Figure 4. A summary of the results is also provided in Table I. It can be seen that H_2 and O_2 cause reconstruction of the Ni surfaces in different ways. These results are consistent with literature results.[33–36]

IV. DISCUSSION

As discussed previously and shown in Figure 3, the MgO substrate is the dominant source of oxygen during annealing. Additionally, there is a significant difference between the measured partial pressure of oxygen under 2310 sccm and 95 sccm flows of 5% H_2 + 95% N_2, as shown in Figure 3. The measured partial pressure of oxygen is 5 orders of magnitude larger for a flow rate of 95 sccm compared to a flow rate of 2310 sccm. This indicates that under the 95 sccm flow, oxygen is more likely to adsorb on the Ni surface, while at 2310 sccm, hydrogen is more likely to adsorb on the sample surface.

As previously mentioned, the surface diffusivity on the top facet of the retracting rim most strongly affects the edge retraction kinetics. In both Ni(110) and Ni(100) films, the top facet of the retracting rim has the same orientation as the macroscopic surface plane of the as-deposited film. To aid further discussion, sketches of reconstructed surface structures of Ni(110) and Ni(100) films under different annealing conditions are provided in Figure 5.

Channels are present in both the O_2 and H_2-induced reconstructions of the Ni(110) surfaces. Diffusivities have been measured for unreconstructed (110) surfaces under vacuum, and diffusivities have been found to be higher in the [001] direction than the [1$\bar{1}$0] direction.[37–39] However, diffusivities on reconstructed surfaces have not been reported. The reconstructed surfaces have relatively wide channels in

TABLE I. Surface structure characteristics for Ni(110) and Ni(100) surfaces under different annealing ambient conditions.

Surface condition	Vacuum	Hydrogen	Oxygen
Reconstructed (110)	1 × 1	1 × 2	2 × 1
Ambient condition	Base P = low 10^{-9} Torr	Surface coverage = 1 langmuir $P(H_2) = 1 \times 10^{-7}$ Torr	Surface coverage = 1 langmuir $P(O_2) = 1 \times 10^{-7}$ Torr
Reconstructed (100)	1 × 1	1 × 1	c(2 × 2)
Ambient condition	Base P = low 10^{-9} Torr	Surface coverage = 1 langmuir $P(H_2) = 1 \times 10^{-7}$ Torr	Surface coverage = 1 langmuir $P(O_2) = 1 \times 10^{-7}$ Torr

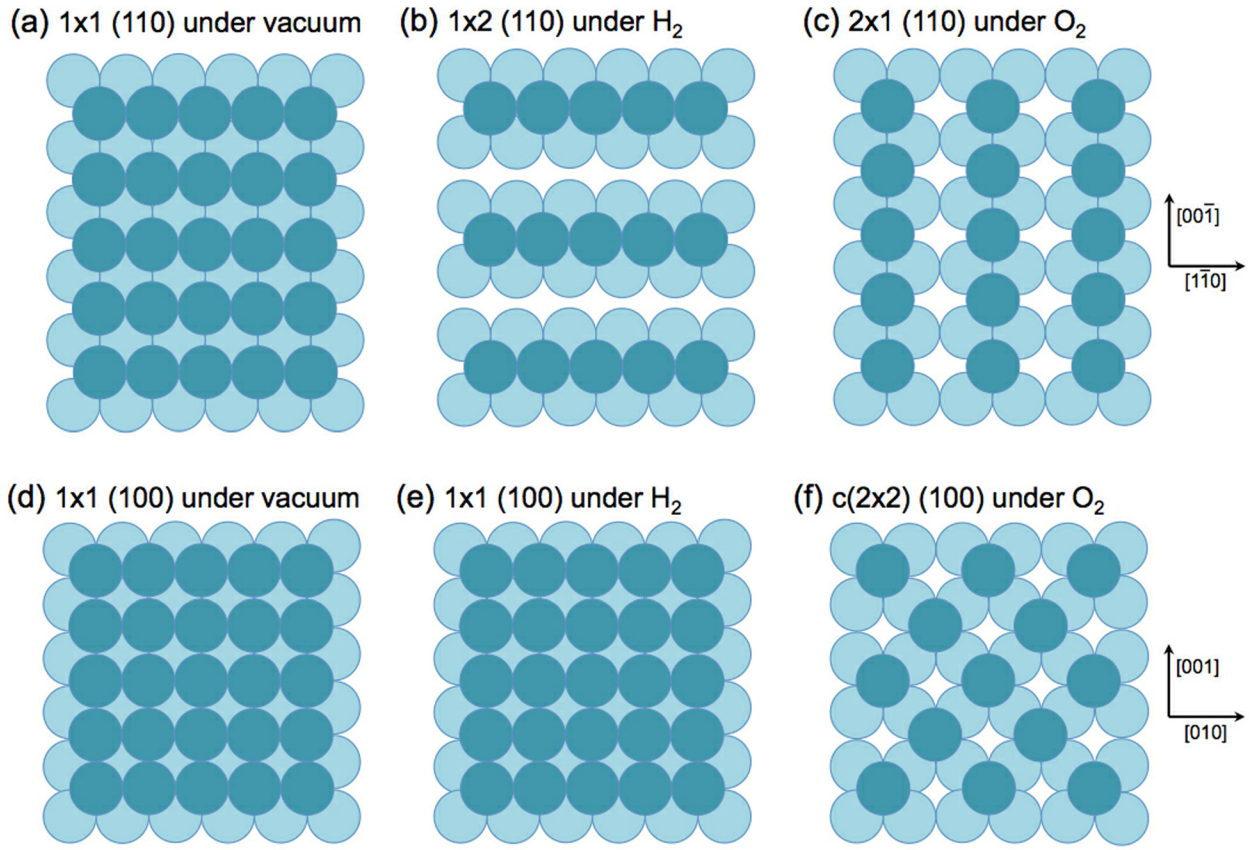

FIG. 5. Surface structures of (a)–(c) Ni(110) and (d)–(f) Ni(100) films under different annealing ambient conditions. The darker spheres are the atoms on the top layer, and the lighter spheres are the atoms underneath the top layer. Details of the annealing conditions are provided in Table I.

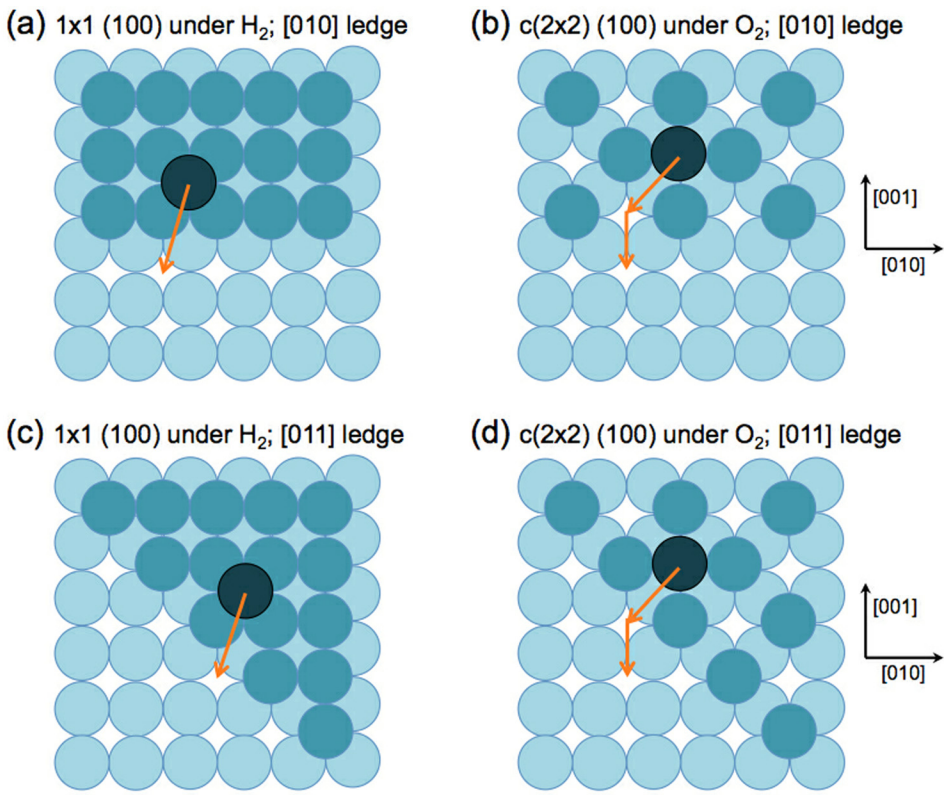

FIG. 6. Illustrations of ledges propagating in different directions for Ni(100) surfaces with different terrace/facet reconstructions. The single darkest sphere indicates an atom diffusing from the uppermost terrace to the adjacent terrace. The second darkest layer of spheres is the uppermost layer of atoms, and the lightest spheres form the layer underneath that layer, as well as the surface atoms of the adjacent terrace. Orange arrows indicate the shortest paths for diffusion of atoms over the ledges.

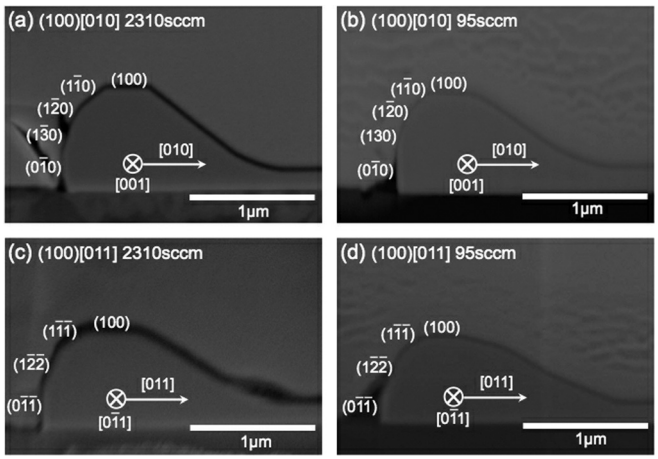

FIG. 7. (a) and (c) Cross-sectional SEM images of retracting rims of kinetically stable edges for Ni(100) films annealed under reducing gas (5% H_2 + 95% N_2) flowing at 2310 sccm. (b) and (d) Cross-sectional SEM images of retracting rims of kinetically stable edges for Ni(100) films annealed under reducing gas (5% H_2 + 95% N_2) flowing at 95 sccm. The images were obtained after a 50-h anneal. The macroscopic retraction direction of the kinetically stable edge and the direction normal to the cross-sectional plane (and parallel to the length of the edge) are also indicated in the individual figures.

different directions, depending on whether the reconstruction is 1×2 or 2×1. It seems reasonable to expect higher Ni self-diffusion rates along these channels. Under H_2 flow, langmuir channels form along the $[1\bar{1}0]$ direction, and under O_2 flow, channels form along the [001] direction. As shown in Figure 1, this change in channel orientation, and the likely changes in fast diffusion directions, is consistent with the observed differences in the relative retraction rates under the different annealing ambient conditions. At a 2310 sccm flow rate of 5% H_2 + 95% N_2, for which H_2 covers the sample surface, retraction in the $[1\bar{1}0]$ direction is faster than in the [001] direction, while at the 95 sccm flow rate of 5% H_2 + 95% N_2, for which O_2 covers the sample surface, the retraction rate in the [001] direction is faster than in the $[1\bar{1}0]$ direction. In addition, as shown in Figure 1, the rate of retraction in the $[1\bar{1}1]$ direction does not significantly differ under the two flow rates. This is because the surface channels do not form along the $[1\bar{1}1]$ direction under either H_2 or O_2 flow.

O_2 causes a $c(2 \times 2)$ reconstruction of the Ni(100) surface, while H_2 does not cause a reconstruction. Interestingly, the in-plane axes of the $c(2 \times 2)$ surface net are rotated by 45° compared to the surface net of the unreconstructed surface (Figures 5(e) and 5(f)). This correlates with the change in the relative retraction rates in the ⟨110⟩ and ⟨100⟩ directions (Figure 1) and changes in the in-plane orientation of growing square holes (insets in Figure 1). However, because the reconstruction remains 4-fold symmetric, the surface diffusivity should remain isotropic. Therefore, correlation of the changes in the orientations of the surface nets and changes in the retraction rate anisotropy cannot be explained simply in terms of relative changes in surface diffusivities.

Even though the observed change in the surface structure does not result in the changes in the isotropy of the surface diffusivity, it can still contribute to the changes in the relative edge retraction kinetics. As edges retract and rims form, the thickness of the rim is observed to increase in dewetting experiments with single crystal Ni[16,21,22] and silicon-on-insulator[18–20] films. It has been observed that during edge retraction in single crystal silicon films, growth of the rim height and advancing of the rim occur through the formation of ledges on the side of the top facet adjacent to the triple line and propagation of the ledges toward the leading edge of the rim. This has been observed in experiments,[20,24,40,41] modeling,[41–44] and simulations.[20,42–45] It is reasonable to expect that this mechanism operates for Ni as well. This requires transport not only across the terrace but also over the edge of a terrace to the adjacent terrace.

Figure 6 illustrates possible differences in the paths for transport of adatoms over ledges with different in-plane orientations for terraces with the two different observed surface structures. The arrows in Figure 6 indicate the shortest diffusion paths. It can be seen that for a given reconstruction the nature of the shortest path is identical for the ledges with different in-plane orientations (compare Figures 6(a) and 6(c), and 6(b) and 6(d)). However, the nearest neighbor environment of the diffusing atoms changes for different ledge orientations. Therefore, it might be expected that the energy that drives diffusion over the ledge changes and that this changes the rate of ledge propagation.

In addition to the changes in the energies that drive adatom motion over ledges, changes in the Ehrlich-Schwoebel barrier[46,47] to diffusion over the edge may also occur. It has been found in other systems that the Ehrlich-Schwoebel barrier for an atom diffusing on a (100) surface over ledges with different in-plane orientations can change due to surface reconstructions on Si(100)[48,49] and GaAs(100)[50] surfaces. It seems likely that changes in the surface structure of Ni(100) can also lead to changes in the Ehrlich-Schwoebel barrier for the ledges associated with kinetically stable edges with different orientations, leading to the observed changes in the relative retraction rates.

Although the rate of diffusion and ledge propagation on the top facet is expected to have the greatest effect on the overall rate of edge retraction, kinetic processes on other facets comprising the retracting rim can also affect the overall retraction kinetics. As shown in Figure 7, many of the facets comprising the rims on edges of Ni(100) films are not 4-fold symmetric, allowing anisotropic diffusivities. For example, the rims that form on the edges retracting in both the [010] and [011] directions for Ni(100) have {110} facets. As has already been discussed, at 2310 sccm, channels form along the $[0\bar{1}1]$ direction on a $(0\bar{1}\bar{1})$ facet. This leads to slower diffusion over the rim in the [011] retraction direction compared to retraction in the [010] direction. On the other hand, at 95 sccm, channels form along the [001] directions on the $(1\bar{1}0)$ facet. This leads to slower diffusion over the rim in the [010] retraction direction, compared to retraction in the [011] direction.

V. SUMMARY AND CONCLUSION

Retraction distances versus annealing times, as a measure of the rate of edge retraction, were determined for kinetically stable edges in single crystal Ni(110) and Ni(100) films. It was found that the edge retraction kinetics is strongly dependent on the flow rates of reducing gases, which change the relative partial pressures of oxygen and hydrogen in the furnace. The

surface structures of Ni(110) and Ni(100) films were characterized both at ultrahigh vacuum and at low vacuum conditions with the presence of low partial pressures of oxygen or hydrogen, and it was found that oxygen and hydrogen induce different reconstructions of the Ni surfaces. These changes in the surface structure were found to correlate with the observed changes in the relative retraction rates of the kinetically stable edges.

The surface reconstructions of Ni(110) films led to channels that are rotated by 90° from a ⟨001⟩ in-plane direction in the presence of O_2 to a ⟨110⟩ in-plane direction in the presence of H_2. It is expected that this leads to the corresponding changes in the direction for fastest surface diffusion, and that this causes the observed change in the relative rates of edge retraction in the [001] and [1$\bar{1}$0] directions. This change in relative retraction rates, in turn, leads to the observed change of the in-plane orientations of growing rectangular holes under 5% H_2 + 95% N_2 reducing gas at high flow rates (for which O_2 is present at very low pressures and H_2 is present at high partial pressures) and under low flow rates (for which O_2 was found to be present at relatively high partial pressures).

The presence of O_2 was found to cause a c(2 × 2) reconstruction of Ni(100) surfaces, while no reconstruction was observed in the presence of H_2. The axes of the square surface nets were found to be rotated by 45° in the two cases. This correlates with relative changes in the rate of edge retraction in ⟨010⟩ and ⟨011⟩ directions and the resulting 45° in-plane rotation of growing square holes under different reducing gas flow rates. However, since four-fold symmetry is retained, so that surface diffusivity isotropy is retained, the observed correlation of the changes in surface structure with changes in relative rates of edge retraction cannot be explained by the changes in the anisotropy of surface diffusion. We argue that the surface reconstruction observed in the presence of O_2 leads to differences in the rate of ledge propagation on the top facets of rims on edges with different in-plane orientations, and that these differences cause changes in the relative edge retraction rates. Changes in the anisotropy of diffusion on other facets on the rims may also contribute to the changes in relative retraction rates.

We have shown that changes in relative edge retraction rates observed under different annealing ambient conditions are correlated with changes in surface reconstructions. The changes in relative retraction rates significantly affect the course of the overall solid-state dewetting process and affect the shapes and orientations of the complex patterns that result from partial dewetting of patterned films. This work therefore provides an improved fundamental understanding of ways in which changes in annealing ambient conditions can be used to control the patterns that are reproducibly formed through templated solid-state dewetting.

ACKNOWLEDGMENTS

This work was supported by the U.S. National Science Foundation through Grant No. DMR-1505947.

[1]C. V. Thompson, Ann. Rev. Mater. Res. **42**(42), 399 (2012).
[2]D. Deduytsche, C. Detavemier, R. L. Van Meirhaeghe, and C. Lavoie, J. Appl. Phys. **98**, 033526 (2005).
[3]C. Jahan, O. Faynot, L. Tosti, and J. M. Hartmann, J. Cryst. Growth **280**, 530 (2005).
[4]R. M. Tiggelaar, R. G. P. Sanders, A. W. Groenland, and J. G. E. Gardeniers, Sens. Actuators, A **152**, 39 (2009).
[5]J. Mizsei, Sens. Actuators, B **16**, 328 (1993).
[6]S. Yang, B. Cao, L. Kong, and Z. Wang, J. Mater. Chem. **21**, 14031 (2011).
[7]S. K. Sardana, V. S. N. Chava, E. T. C. Chander, S. Kumar, S. R. Reddy, and V. K. Komarala, Appl. Phys. Letts. **104**, 073903 (2014).
[8]G. R. Swathilyer, J. Wang, G. Wells, S. Guruvenket, S. Payne, M. Bradley, and F. Borondics, ACS Nano **8**, 6353 (2014).
[9]A. B. Tesler, L. Chuntonov, T. Karakouz, T. A. Bendikov, G. Haran, A. Vaskevich, and I. Rubinstein, J. Phys. Chem. C **115**, 24642 (2011).
[10]C. Eminian, F.-J. Haug, O. Cubero, X. Niquille, and C. Ballif, Prog. Photovoltaics **19**, 260 (2011).
[11]S. Morawiec, M. J. Mendes, S. A. Filnovich, T. Mateus, S. Mirabella, H. Aguas, I. Ferreira, F. Simone, E. Fortunato, R. Martins, F. Priolo, and I. Crupi, Opt. Express **22**, A1059 (2014).
[12]J. E. Yoo, K. Lee, M. Altomare, E. Selli, and P. Schmuki, Angew. Chem. **52**, 7514 (2013).
[13]D. J. Srolovitz and S. A. Safran, J. Appl. Phys. **60**, 255 (1986).
[14]H. Wong, P. W. Voorhees, M. J. Miksis, and S. H. Davis, Acta Mater. **48**, 1719 (2000).
[15]J. Ye and C. V. Thompson, Phys. Rev. B **82**, 193408 (2010).
[16]G. H. Kim, R. Zucker, J. Ye, W. C. Carter, and C. V. Thompson, J. Appl. Phys. **113**, 043512 (2013).
[17]Y. Ono, M. Nagase, M. Tabe, and Y. Takahashi, Jpn. J. Appl. Phys., Part 1 **34**, 1728 (1995).
[18]P. Sutter, W. Ernst, Y. S. Choi, and E. Sutter, Appl. Phys. Lett. **88**, 141924 (2006).
[19]R. Nuryadi, Y. Ishikawa, and M. Tabe, Appl. Surf. Sci. **159–160**, 121 (2000).
[20]F. Cheynis, E. Bussmann, F. Leroy, T. Passanante, and P. Mueller, Phys. Rev. B **84**, 245439 (2011).
[21]J. Ye and C. V. Thompson, Appl. Phys. Lett. **97**, 071904 (2010).
[22]J. Ye and C. V. Thompson, Acta Mater. **59**, 582 (2011).
[23]D. Amram, L. Klinger, and E. Rabkin, Acta Mater. **60**, 3047 (2012).
[24]F. Leroy, F. Cheynis, T. Passanante, and P. Mueller, Phys. Rev. B **85**, 195414 (2012).
[25]M. Eriksson, L. Olsson, U. Helmersson, R. Erlandsson, and L. G. Ekedahl, Thin Solid Films **342**, 297 (1999).
[26]A. E. B. Presland, G. L. Price, and D. L. Trimm, Prog. Surf. Sci. **3**, 63 (1972).
[27]A. Kosinova, O. Kovalenko, L. Klinger, and E. Rabkin, Acta Mater. **83**, 91 (2015).
[28]R. V. Zucker, G. H. Kim, W. C. Carter, and C. V. Thompson, C. R. Phys. **14**, 564 (2013).
[29]J. M. Blakely and H. Mykura, Acta Metall. **9**, 595 (1961).
[30]R. T. Tung and W. R. Graham, Surf. Sci. **97**, 73 (1980).
[31]C. M. Chang, C. M. Wei, and J. Hafner, J. Phys.: Condens. Matter **13**, L321 (2001).
[32]R. H. Lamoreaux, D. L. Hildenbrand, and L. Brewer, J. Phys. Chem. Ref. Data **16**, 419 (1987).
[33]K. Christmann, G. Ertl, and O. Schober, Surf. Sci. **40**, 61 (1973).
[34]W. Oed, H. Lindner, U. Starke, K. Heinz, and K. Muller, Surf. Sci. **224**, 179 (1989).
[35]L. H. Germer and A. U. MacRae, J. Chem. Phys. **37**, 1382 (1962).
[36]K. Baberschke, U. Dobler, L. Wenzel, and D. Arvanitis, Phys. Rev. B **33**, 5910 (1986).
[37]P. S. Maiya and J. M. Blakely, J. Appl. Phys. **38**, 698 (1967).
[38]E. E. Latta and H. P. Bonzel, Phys. Rev. Lett. **38**, 839 (1977).
[39]H. P. Bonzel and E. E. Latta, Surf. Sci. **76**, 275 (1978).
[40]F. Leroy, F. Cheynis, T. Passanante, and P. Muller, Phys. Rev. B **88**, 035306 (2013).
[41]F. Cheynis, F. Leroy, and P. Muller, C. R. Phys. **14**, 578 (2013).
[42]O. Pierre-Louis, A. Chame, and M. Dufay, Eur. Phys. J. B **77**, 57 (2010).
[43]O. Pierre-Louis, A. Chame, and Y. Saito, Phys. Rev. Lett. **103**, 195501 (2009).
[44]A. Chame and O. Pierre-Louis, C. R. Phys. **14**, 553 (2013).
[45]E. Bussmann, F. Cheynis, F. Leroy, P. Muller, and O. Pierre-Louis, New J. Phys. **13**, 043017 (2011).
[46]G. Ehrlich and F. G. Hudda, J. Chem. Phys. **44**, 1039 (1966).
[47]R. L. Schwoebel and E. J. Shipsey, J. Appl. Phys. **37**, 3682 (1966).
[48]W. Hong, Z. Zhang, and Z. Suo, Phys. Rev. B **74**, 235318 (2006).
[49]W. Hong, Z. Suo, and Z. Zhang, J. Mech. Phys. Solids **56**, 267 (2008).
[50]Y. B. Zheng, S. J. Chua, C. H. A. Huan, and Z. L. Miao, J. Cryst. Growth **263**, 161 (2004).